frontiers in Earth Science

ORIGINAL RESEARCH
published: 27 January 2022
doi: 10.3389/feart.2022.828801

A ~28-kyr Continuous Lacustrine Paleoseismic Record of the Intraplate, Slow-Slipping Fuyun Fault in Northwest China

Jiawei Fan[1,2,3], Hongyan Xu[1], Wei Shi[1], Qiaoqiao Guo[1], Siqi Zhang[1], Xiaotong Wei[1], Minggang Cai[1], Shuaitang Huang[4], Jiangyong Wang[5] and Jule Xiao[6,7,8]*

[1]State Key Laboratory of Earthquake Dynamics, Institute of Geology, China Earthquake Administration, Beijing, China, [2]Xinjiang Pamir Intracontinental Subduction National Field Observation and Research Station, Beijing, China, [3]Urumqi Institute of Central Asia Earthquake, China Earthquake Administration, Urumqi, China, [4]Earthquake Agency of Xinjiang Uygur Autonomous Region, Urumqi, China, [5]College of Urban and Environmental Science, Northeast Normal University, Changchun, China, [6]CAS Key Laboratory of Cenozoic Geology and Environment, Institute of Geology and Geophysics, Chinese Academy of Sciences, Beijing, China, [7]CAS Center for Excellence in Life and Paleoenvironment, Beijing, China, [8]College of Earth and Planetary Sciences, University of Chinese Academy of Sciences, Beijing, China

OPEN ACCESS

Edited by:
Chong Xu,
Ministry of Emergency Management, China

Reviewed by:
Qi Yao,
China Earthquake Administration, China
Xiangli He,
China Earthquake Administration, China

***Correspondence:**
Jiawei Fan
jwfan@ies.ac.cn

Specialty section:
This article was submitted to Geohazards and Georisks, a section of the journal Frontiers in Earth Science

Received: *04 December 2021*
Accepted: *10 January 2022*
Published: *27 January 2022*

Citation:
Fan J, Xu H, Shi W, Guo Q, Zhang S, Wei X, Cai M, Huang S, Wang J and Xiao J (2022) A ~28-kyr Continuous Lacustrine Paleoseismic Record of the Intraplate, Slow-Slipping Fuyun Fault in Northwest China. Front. Earth Sci. 10:828801. doi: 10.3389/feart.2022.828801

The Fuyun Fault is a typical intraplate, slow-slipping fault, but has been repeatedly ruptured by surface wave magnitude (M_S) ≥ 8.0 earthquakes. The 11 August 1931 M_S 8.0 Fuyun earthquake resulted in more than 10,000 casualties in the sparsely populated Fuyun area. Cosmogenic ^{10}Be dating of offset landforms produced by prehistoric M_S ≥ 8.0 earthquakes yields an average recurrence interval of 9,700 ± 3,300 years, much longer than previously estimated 2,000–4,500 years, clouding our understanding of the timing and recurrence behavior of past earthquakes originating from the Fuyun Fault. Reflection seismic data reveal widely distributed subaquatic faults in Yileimu Lake, implying high sensitivity of the lake sediments to paleoearthquakes originating from the Fuyun Fault. Two new long sediment cores (Y20A: 267 cm; Y20B: 890 cm) together with previously published two short cores (Y19: 71 cm; Y20: 31.5 cm) from the depocenter and nearshore zone of Yileimu Lake are used for stratigraphic correlations and analyses of sedimentary structures, grain-size distributions, magnetic susceptibility, elemental composition and carbon content. The mass-wasting deposits with underlying soft-sediment deformation structures (SSDS) in the Y20B core indicate six siliciclastic-enriched sandy sediment fluxes from earthquake-triggered landslides of granitic rocks, and isolated SSDS record three additional earthquake-induced *in situ* deformations. Turbidite-like deposits with sorting indices >3 and Si contents >700 counts per second (cps) are comparable to those of the seismic mass-wasting deposits, and are thus interpreted as seismites from earthquake-induced re-deposition of nearshore sediments. There are a total of 20 seismic events recorded by the Y20B core. Seismic intensity calculation results, combined with historical seismic data, provide potential magnitudes of M_S ≥ 8.0, M_S ≥ 7.0, and M_S ≥ 5.5 for the earthquake-triggered mass-wasting deposits, SSDS, and turbidite-like seismites, respectively, in Yileimu Lake, generally consistent with previously published magnitude thresholds. Radiocarbon dating and stratigraphic correlations constrain the timing of these past earthquakes to

~28 cal kyr BP. This unique, long lacustrine paleoseismic record suggests a weakly periodic pattern with recurrence intervals between 2,317 and 7,830 years and an average of 5,303 years for potential $M_S \geq 8.0$ earthquakes, and reveals an unprecedented high frequency of potential $M_S \geq 7.0$ earthquakes originating from the Fuyun Fault in the last 5 kyr, demonstrating the urgent need for an improved assessment of seismic hazards and risks in the Fuyun Fault zone.

Keywords: mass-wasting deposits, soft-sediment deformations, turbidite, shaking intensity, recurrence behavior, intraplate fault

INTRODUCTION

In recent decades, the frequent occurrence of catastrophic earthquakes (e.g., the 17 August 1999 M_s 7.4 earthquake in Turkey, the 8 October 2005 M_s 7.6 earthquake in Pakistan, and the 12 May 2008 M_s 8.0 earthquake in China) produced by sudden stress release of intraplate active faults have resulted in massive casualties, property loss and ecological destruction (Vanholder et al., 2001; Sullivan and Hossain, 2010; Cui et al., 2012). The Fuyun Fault is a typical intraplate fault located at the junction of Tianshan–Altay and Mongolia–Baikal seismic zones, an area with frequent large earthquakes (Pollitz et al., 2003). A rupture along the ~170-km long Fuyun Fault produced the 11 August 1931 M_s 8.0 Fuyun earthquake with a maximum horizontal coseismic displacement of ~14 m. It resulted in more than 10,000 casualties, causing great trauma to the sparsely populated Fuyun area (Fuyun County Local Chronicles Compilation Committee, 2003). The Fuyun Fault is a slow-slipping fault but evidence indicates that it ruptured repeatedly generating prehistoric $M_s \geq 8.0$ earthquakes (Klinger et al., 2011; Xu et al., 2012). Mapping of the Fuyun Fault offsets using satellite and geomorphological data and cosmogenic ^{10}Be dating of the offset landforms yielded an average recurrence interval of 9,700 ± 3,300 years for the prehistoric earthquakes (Xu et al., 2012). However, such a long recurrence interval is in sharp contrast with the previously estimated interval of 2,000–4,500 years in Xinjiang active tectonic zones (Xu and Deng, 1996).

The short instrumental and historical earthquake records in the Fuyun area is insufficient to determine the long-term recurrence behavior of devastating earthquakes from such intraplate faults (Avşar et al., 2014; Howarth et al., 2014; Moernaut, 2020). Quaternary deposits in the Altay region are sporadic, limiting the investigation of paleoseismic trenches for the Fuyun Fault. Dendroseismological studies can provide absolute ages for past earthquakes associated with the Fuyun Fault (Lin and Lin, 1998). However, seismic intensity thresholds for tree-ring responses are poorly constrained in the fault area due to the scarcity of historical earthquake events (e.g., Fan et al., 2020a), and dendrochronological studies may be limited to a much shorter time span than the long return periods of multiple great earthquakes. Therefore, paleoseismic records with a long time span and containing information regarding earthquake size are urgently needed to gain a better understanding of seismic activities on the Fuyun Fault.

Continuously deposited lake sediments in fault-bounded basins potentially contain detailed information on the occurrence and age of paleoearthquake events (e.g., Strasser et al., 2006; Berryman et al., 2012; Hubert-Ferrari et al., 2020; Kremer et al., 2020; Moernaut, 2020; Oswald et al., 2021). Previous lacustrine paleoseismic studies have provided some intensity thresholds for earthquake-induced sedimentary and deformation processes: a Modified Mercalli Intensity (MMI) of 5–6 induced turbidite deposition in Rara Lake, western Nepal (Ghazoui et al., 2019); an intensity of 6–7 MMI produced soft-sediment deformation structures (SSDS) in Lungerer Lake, Seelisberg Lake and Baldegger Lake, central Switzerland (Monecke et al., 2004); and a violent shaking intensity of 9 MMI caused extensive landslides and triggered mass-wasting deposits in Mapourika Lake, Paringa Lake and Ellery Lake, New Zealand (Howarth et al., 2016). The intensity thresholds for earthquake-induced lacustrine sedimentary events provide a means to investigate the location and magnitude of past earthquakes and to determine the recurrence pattern of earthquake events of different intensities (Moernaut et al., 2018; Lu et al., 2020).

Yileimu Lake is bounded by the Fuyun Fault (**Figure 1A**), making this site particularly sensitive to seismic activities originating from the fault. A recent study based on a 71-cm long sediment core from Yileimu Lake provided a 450-years continuous paleoseismic record related to the Fuyun Fault (Fan et al., 2020b). Here, we present an extended history of this paleoseismic record to ~28 cal kyr BP, through high-resolution analyses of chronology and sedimentary events including mass-wasting deposits, SSDS and turbidite-like deposits in an 890-cm long sediment core from Yileimu Lake, and through careful statistical analysis of grain-size data, and elemental composition. The sedimentary events in this unique, long paleoseismic record are constrained by different shaking intensities, providing an in-depth understanding of the magnitude, frequency and recurrence behavior of past earthquakes on the Fuyun Fault since ~28 cal kyr BP.

MATERIALS AND METHODS

Study Area

The Fuyun Fault is a ~170-km long intraplate strike-slip fault in southern Altay, northern Xinjiang, which is on the border of China, Mongolia and Russia (**Figure 1A**). It consists of two segments: one is a ~50 km-long normal fault, constituting the northern segment; the other is a ~120 km-long right-lateral slip

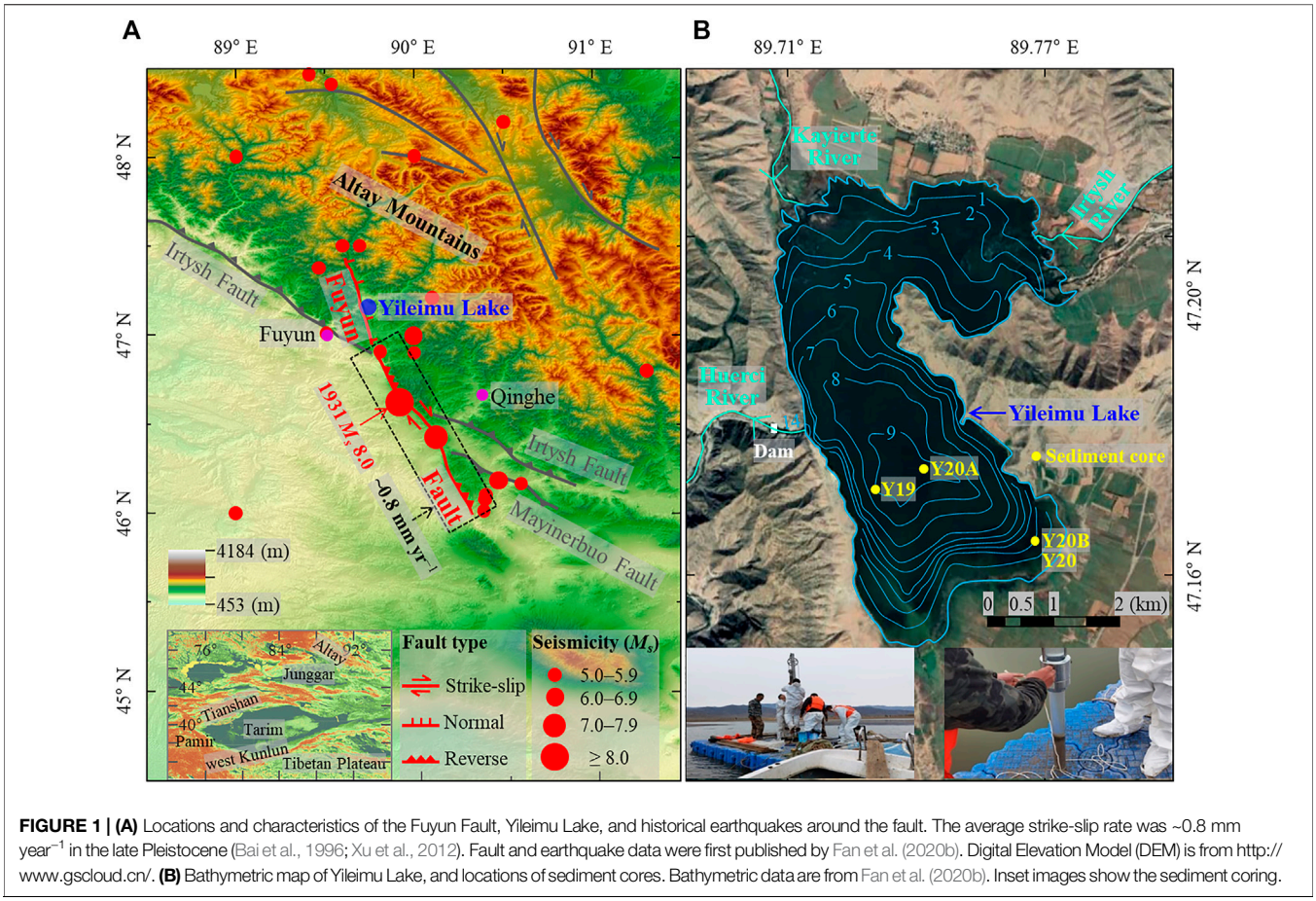

FIGURE 1 | (A) Locations and characteristics of the Fuyun Fault, Yileimu Lake, and historical earthquakes around the fault. The average strike-slip rate was ~0.8 mm year^{-1} in the late Pleistocene (Bai et al., 1996; Xu et al., 2012). Fault and earthquake data were first published by Fan et al. (2020b). Digital Elevation Model (DEM) is from http://www.gscloud.cn/. **(B)** Bathymetric map of Yileimu Lake, and locations of sediment cores. Bathymetric data are from Fan et al. (2020b). Inset images show the sediment coring.

fault with a thrust component, constituting the southern segment (**Figure 1A**) (Ding, 1985; Klinger et al., 2011; Xu et al., 2012). The southern segment of the fault is more active, in response to the southeastward movement of the Mongolia and Siberia blocks and to the far-field effect of India-Eurasia collision (Shen et al., 2003). The average strike-slip rate was ~0.8 mm year^{-1} in the late Pleistocene (Bai et al., 1996; Xu et al., 2012). Historical earthquake records cover only 120 years, but document an M_s 8.0 earthquake that ruptured the whole Fuyun Fault and triggered extensive landslides in 1931 AD (**Figure 1A**) (Fuyun County Local Chronicles Compilation Committee, 2003).

Yileimu Lake is a permanent lake formed by depression of the northern segment of the Fuyun Fault (Klinger et al., 2011). It is fed by the Kayierte and Irtysh Rivers and is discharged by the Huerci River (**Figure 1B**). The current lake level is mainly controlled by an artificial dam (20.8 m above the ground) located ~0.5 km downstream along the Huerci River (**Figure 1B**). The dam was built in 1958–1967 AD (Fuyun County Local Chronicles Compilation Committee, 2003). Yileimu Lake has a maximum water depth of ~9 m in the depocenter, and the lake floor is flat in the north and relatively steep in the south (**Figure 1B**) (Fan et al., 2021). Hills of granitic rocks with an average slope of ~35° occur along the Fuyun Fault, bounding the western margin of the lake (**Figures 1A,B**, **Supplementary Figure S1A**). The lake is surrounded by lacustrine plains along the northern, northeastern, southeastern and southern shores (**Figure 1B**). The catchment area has ~300 m of relief between the mountain peaks and lake surface, and landslides appear on the slopes to the southwest of the lake. Chemical weathering is relatively weak in the Altay Mountains, limiting the sediment sources for the lake to some extent (Fan et al., 2021).

Reflection Seismic Survey and Sediment Coring

A reflection seismic survey was conducted along nine seismic lines across Yileimu Lake in May 2021 (only three lines A, B and C in **Supplementary Figure S1A** have relatively clear seismic reflectors). Reflection seismic data were acquired using an Applied Acoustics Engineering (AAE) CSP–D2400 system in combination with a GeoAcoustics 5210A system. A Receiver Model 5210A was used to collect seismic data from an AA301 boomer seismic sound source (200 J) and a 20-unit hydrophone (100–4,000 Hz), and to collect differential Global Positioning System (DGPS) data. A band-pass filter of 200–15,000 Hz was applied and seismic data interpretation was performed using SonarWiz 7 (v7.07.04) software.

In September 2020, a 267-cm long sediment core (Y20A; 47.176°N, 89.740°E) and an 890-cm long sediment core (Y20B; 47.165°N, 89.764°E) were retrieved from the depocenter (at a

TABLE 1 | Accelerator Mass Spectrometry (AMS) ^{14}C ages for the Y20A and Y20B cores.

Laboratory number	Depth (cm)	Dating material	$\delta^{13}C$ (‰)	Conventional ^{14}C age (year BP)	Corrected ^{14}C age[a] (year BP)	Calibrated ^{14}C age (2σ) (cal year BP)
NENUR11114[b]	Core top[c]	Organic matter	−19.1	890 ± 30		−70[d]
NENUR11115[b]	45[c]	Organic matter	−14.3	8,800 ± 60[e]	3,070 ± 70	3,125–3,496
Beta–597772[f]	50[c]	Organic matter	−21.1	8,820 ± 30[e]	3,090 ± 35	3,261–3,435
NENUR11118[b]	200[c]	Organic matter	−18.2	13,600 ± 100[e]	7,870 ± 105	8,504–9,046
NENUR11120[b]	375[c]	Organic matter	−17.7	16,460 ± 150[e]	10,730 ± 155	12,224–13,135
Beta–597774[f]	450[c]	Organic matter	−19.9	24,270 ± 80		
Beta–558775[f]	650[c]	Organic matter	−20.8	20,110 ± 60[e]	14,380 ± 70	17,377–17,885
Beta–558776[f]	850[c]	Organic matter	−20.7	15,340 ± 50		
NENUR11111[b]	198[g]	Branch	−21.5	3,090 ± 35[e]	3,090 ± 35	3,261–3,435
NENUR11113[b]	264[g]	Wood	−23.6	3,180 ± 35[e]	3,180 ± 35	3,327–3,511

[a]*The reservoir-corrected ^{14}C ages. The reservoir correction factor is 5,730 years for the Y20B core (see main text for interpretation).*
[b]*NENUR: State Key Laboratory of Organic Geochemistry, Guangzhou Institute of Geochemistry, Chinese Academy of Sciences.*
[c]*Samples from the Y20B core.*
[d]*Sampling date.*
[e]*Age data used in the age–depth model of the Y20B core.*
[f]*Beta: Beta Analytic Testing Laboratory, Beta Analytic Inc, 4985 SW 74th Court Miami, Florida 33155.*
[g]*Samples from the Y20A core. The depths of 50 and 72 cm of the Y20B core correspond to the depths of 198 and 264 cm of the Y20A core, respectively (see main text for interpretation).*

water depth of 9.21 m) and nearshore zone (at a water depth of 2.00 m) of Yileimu Lake, respectively (**Figure 1B**), using a Wink S5 sonic drill system (Canada). The sediment cores had a diameter of 55 mm. The nearest offshore distances of the Y20A and Y20B cores were ~1.2 and ~0.4 km, respectively (**Figure 1B**). The Y20A and Y20B cores were split for X-ray fluorescence scanning, and then sampled at 0.5-cm intervals for physical and chemical analyses. In addition, a 31.5-cm long sediment core (Y20) was retrieved near the Y20B core, and a 71-cm long sediment core (Y19; 47.175°N, 89.729°E) was retrieved from the depocenter of the lake (**Figure 1B**), using a UWITEC gravity corer (Austria). The lithology, chronology and grain-size data from the Y19 (which was named "Y19B" in the previous study of Fan et al. 2020b) and Y20 cores were published (Fan et al., 2021) and are used for stratigraphic correlations in this study.

Accelerator Mass Spectrometry (AMS) Radiocarbon Dating

A total of eight bulk samples from organic-rich horizons of the Y20B core, plus one branch sample at 223 cm depth and one wood sample at 264 cm depth within the Y20A core, were selected for AMS ^{14}C dating. This was carried out at the Guangzhou Institute of Geochemistry, Chinese Academy of Sciences and the Beta Analytic Testing Laboratory, United States (**Table 1**). Organic matter from bulk samples was extracted through an AAA pretreatment process (washing with acid, alkali and acid) (Brock et al., 2010). Conventional ^{14}C ages were calibrated using the OxCal 7.1 calibration program (Bronk Ramsey and Lee, 2013) with IntCal20 calibration data (Reimer et al., 2020). An age–depth profile was constructed using a Bayesian Accumulation Model (Blaauw and Christen, 2011).

X-Ray Fluorescence (XRF) Scanning

One half of each of the Y20A and Y20B cores was smoothed, and then scanned on an Itrax core scanner. Radiographic images were scanned at a resolution of 0.1 cm, using an Rh tube at 60 kV voltage and 35 mA current. Relative element intensities were obtained at 30 kV voltage and 55 mA current with an exposure time of 3 s for every 0.5 cm. Principal component analysis (PCA) was conducted on the standardized proxy data (Si, K, Ti, Fe, Zr, Al, Mn, Ca, Rb, Sr) of the Y20B core, using the software SPSS (Fan et al., 2016), in order to discriminate different sedimentary facies associated with different sedimentary processes, based on their distinguishable compositional characteristics (Praet et al., 2020; Wils et al., 2021). The main factor values (PCA F1 and F2) for each sample were calculated following the method of Fan et al. (2016).

Analyses of Grain-Size Distributions and Magnetic Susceptibility (SUS)

A total of 534 samples from the Y20A core and 1780 samples from the Y20B core were used for grain-size distribution analysis, and the Y20B core was also used for analysis of magnetic susceptibility. Grain-size data were measured using a Malvern Mastersizer 3000 laser grain-size analyzer, and SUS data were measured using a Bartington MS2 susceptibility meter at the Institute of Geology, China Earthquake Administration, following the method of Fan et al. (2020b). The Mastersizer 3000 automatically outputs the volume percentage of 100 grain-size fractions. Sorting index of each grain-size distribution was calculated using the GRADISTAT program (Blott and Pye, 2001). SUS values were normalized by the sample weight.

Analysis of Total Inorganic Carbon (TIC) Content

The Y20B core was sampled at 5-cm intervals (178 samples) for analysis of TIC content, using an Elementar Rapid CS Cube analyzer at the Institute of Geology, China Earthquake Administration. Each sample was separated into two subsamples. One subsample was used for the measurement of total carbon (TC) content, and the other was pretreated with 1 M

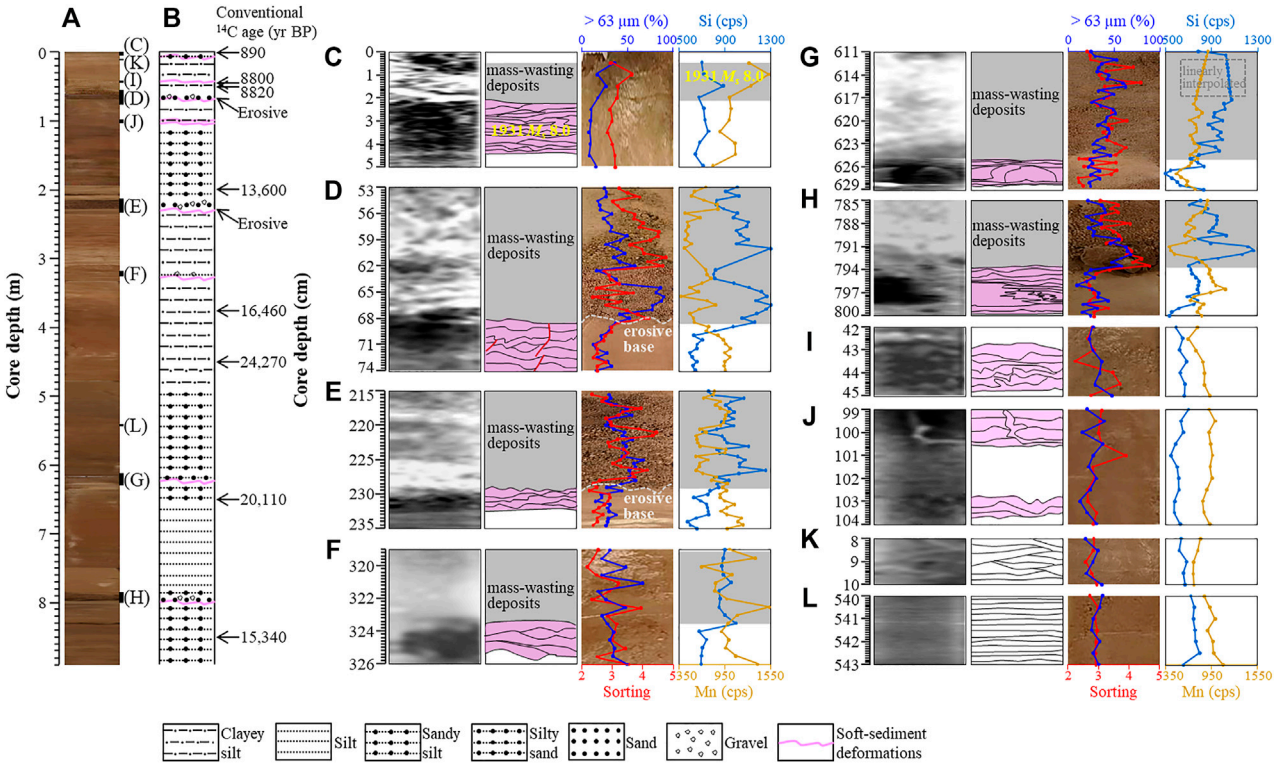

FIGURE 2 | (A) Optical image and **(B)** lithology and conventional ^{14}C ages of the Y20B core. **(C–H)** Soft-sediment deformation structures (SSDS) from radiographic images of the Y20B core, with overlying sandy deposits (mass-wasting deposits). **(C,E,F)** Linear waves. **(D)** Micro-faults. **(G)** Convolute structures. **(H)** Linear waves and clastic dykes. The mass-wasting deposits are generally characterized by high sand percentages, sorting indices and Si contents, and relatively low Mn contents. Note that the sedimentary structures are not clear in optical images, potentially due to the low sedimentation rates. Sharp erosive bases can be found at the interfaces of typical mass-wasting deposits and the underlying SSDS in **(D,E)**. The mass-wasting deposits overlying the SSDS in **(C)** are related to the 11 August 1931 M_S 8.0 Fuyun earthquake. **(I,J)** Isolated SSDS without overlying mass-wasting deposits. **(I)** Linear waves. **(J)** A clastic dyke (upper) and linear waves (lower). **(K)** Cross bedding. **(L)** Horizontal laminations (background sediments). Cps, counts per second. High sorting indices indicate poor sorting of sediments.

HCl to remove carbonates and then used for the measurement of total organic carbon (TOC) content, following the method of Fan et al. (2020b). TIC content was calculated as the difference between the TC and TOC contents.

RESULTS

Seismic Stratigraphy and Core Lithology

Seismic profiles from three lines across Yileimu Lake cover a maximum sediment depth of ~15 m (**Supplementary Figures S1A–D**). The poor penetration of seismic reflection may be related to the presence of highly reflective sediments such as coarse gravels (Wils et al., 2021). Nevertheless, several subaquatic faults are clearly imaged by reflection offsets and changes in reflector characteristics in the same horizons (**Supplementary Figures S1B–D**). In contrast to subaquatic faults, river channels are characterized by a grooved shape without lithological differences of the same horizons (**Supplementary Figure S1C**).

The Y20B core is close to a subaquatic fault in the southeast of Yileimu Lake (**Supplementary Figure S1B**). It generally consists of a continuous lacustrine sequence. The sediments can be divided into six units (**Figures 2A,B**): 890–775 cm, greyish-brown sandy silt with coarse sand and scattered gravel at 793.5–790 cm; 775–650 cm, brown silt; 650–495 cm, brown sandy silt with silty sand at 624.5–611.5 cm; 495–240 cm, brown clayey silt with silt and scattered gravel at 323.5–319 cm; 240–110 cm, greyish-brown sandy silt with sand and scattered gravel at 228–215.5 cm; 110–0 cm, greyish-brown clayey silt with sand and scattered gravel at 68.5–53 cm and sandy silt at 2–0 cm.

The Y20A core can be divided into two units (**Supplementary Figure S2**): 267–160 cm, brownish-grey silty sand with coarse gravel and abundant plant residues at 267–260 cm, plus coarse sand and scattered fine gravel at 260–254 cm; 160–0 cm, greenish-grey clayey silt with occasional black bands. The occurrence of coarse gravel at the bottom of the Y20A core hinders access to longer sediment cores in the depocenter of Yileimu Lake.

AMS Radiocarbon Ages of Sediment Cores

The conventional ^{14}C age of organic matter from the top of the Y20B core is 890 ± 30 years BP, much older than the sampling date (**Figure 2B**; **Table 1**). The age data from the upper 450 cm of the Y20B core are generally consistent with stratigraphic order (**Figure 2B**; **Table 1**). The ^{14}C ages of organic matter at the depths of 45, 50, 200, 375 and 450 cm of the Y20B core are 8,800 ± 60,

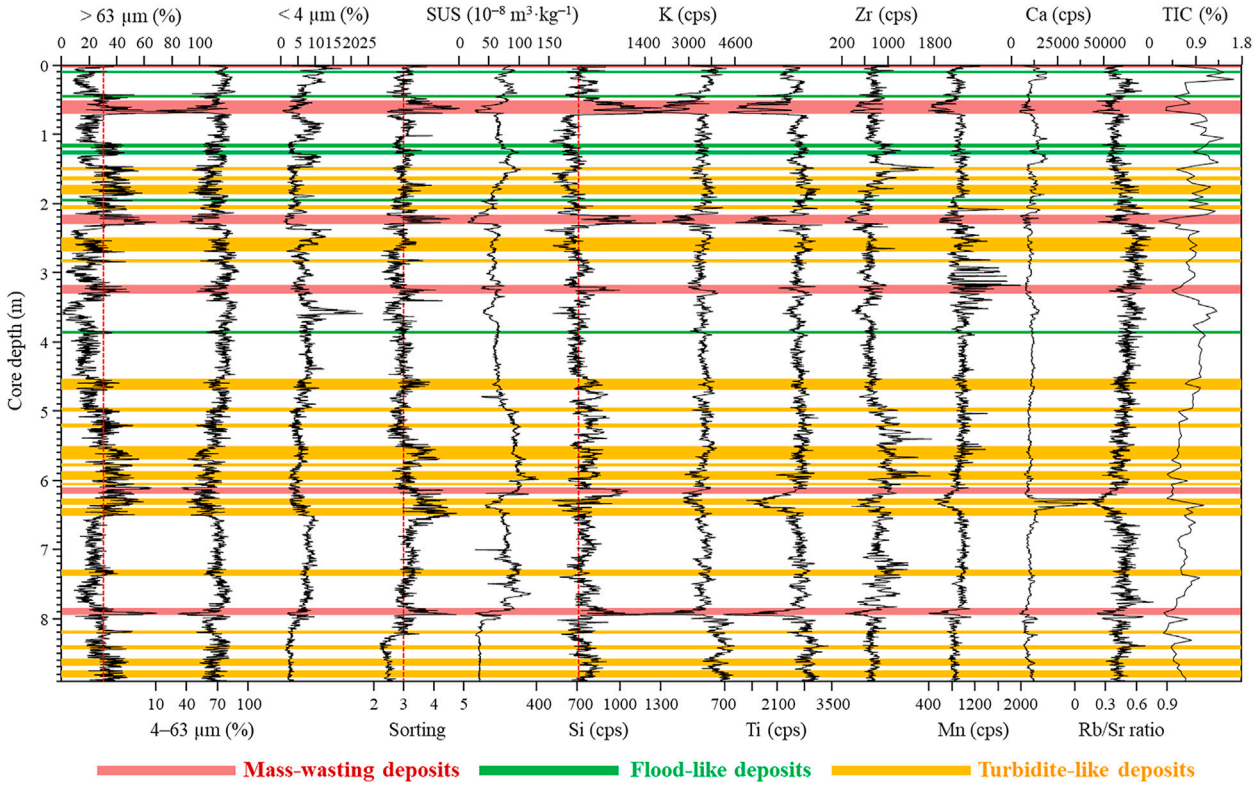

FIGURE 3 | Percentages of >63, 4–63 and <4 μm fractions, sorting index, magnetic susceptibility (SUS), major elemental contents, Rb/Sr ratio and total inorganic carbon (TIC) of the Y20B core. Red, green and yellow bars indicate the horizons of mass-wasting deposits (corresponding to **Figures 2C–H**), flood-like deposits and turbidite-like deposits, respectively. Flood-like deposits have cross bedding structures and turbidite-like deposits generally have normally graded bedding sequences.

8,820 ± 30, 13,600 ± 100, 16,460 ± 150 and 24,270 ± 80 year BP, respectively (**Figure 2B**; **Table 1**). Organic matter from the depth of 850 cm within the Y20B core has a ^{14}C age of 15,340 ± 50 years BP, much younger than the age of 20,110 ± 60 years BP found at 650 cm (**Figure 2B**; **Table 1**). The branch and wood from the depths of 198 and 264 cm of the Y20A core have conventional ^{14}C ages of 3,090 ± 35 and 3,180 ± 35 years BP, respectively (**Supplementary Figure S2**; **Table 1**).

Sedimentary Structures From XRF Radiographic Images

Sedimentary structures are obtained from painstaking searches of radiographic and optical images at 0.1-cm intervals throughout the Y20B and Y20A cores. The Y20B core contains 9 horizons of soft-sediment deformation structures (SSDS; **Figures 2C–J**), and six horizons of mass-wasting deposits overlying the SSDS (**Figures 2C–H**). The SSDS are 1–6.5 cm in thickness, and consist mainly of clayey silt (**Figures 2C,I,J**) and sandy silt (**Figures 2D–H**). They include linear waves (**Figures 2C,E,F,I,J**), micro-faults (**Figure 2D**), a liquefied diaper or convolute structures (**Figure 2G**), linear waves and clastic dykes (**Figure 2H**), and a clastic dyke (**Figure 2J**). The mass-wasting deposits are generally composed of poorly sorted medium- to coarse-sand with a massive structure and scattered gravel dispersed in (red bars in **Figure 3**). They are 2 cm (**Figure 2C**), 15.5 cm (**Figure 2D**), 14.5 cm (**Figure 2E**), 4 cm (**Figure 2F**), 13.5 cm (**Figure 2G**) and 8.5 cm (**Figure 2H**) in thickness, respectively. Except for the mass-wasting deposits at 624.5–611 cm depths, the others generally have normally graded sequences and clear lithological interfaces with the underlying SSDS (**Figures 2C–H**). There are no Bouma divisions, no horizontal or cross bedding, and no signs of bioturbation in the mass-wasting deposits. Sharp erosive bases can be found at the interfaces of typical mass-wasting deposits and the underlying SSDS (**Figures 2D,E**). The sediments consisting of sandy silt with clear cross-bedding structures and normally graded bedding sequences in the Y20B core are regarded as flood-like deposits (**Figure 2K**). The flood-like deposits are well sorted, and are less than 7 cm in thickness (green bars in **Figure 3**). In contrast, the sediments consisting of normally graded sandy silt without cross-bedding structures are regarded as turbidite-like deposits. The turbidite-like deposits have a wide range of thickness (1–19.5 cm) (yellow bars in **Figure 3**). The background sediments in the Y20B core mainly comprise laminated silt without graded sequences (e.g., **Figure 2L**). The Y20A core contains a horizon of mass-wasting deposits at 267–254 cm and a horizon of isolated SSDS layers (linear waves and convolute structures) at 171.7–168.2 cm (**Supplementary Figure S2**).

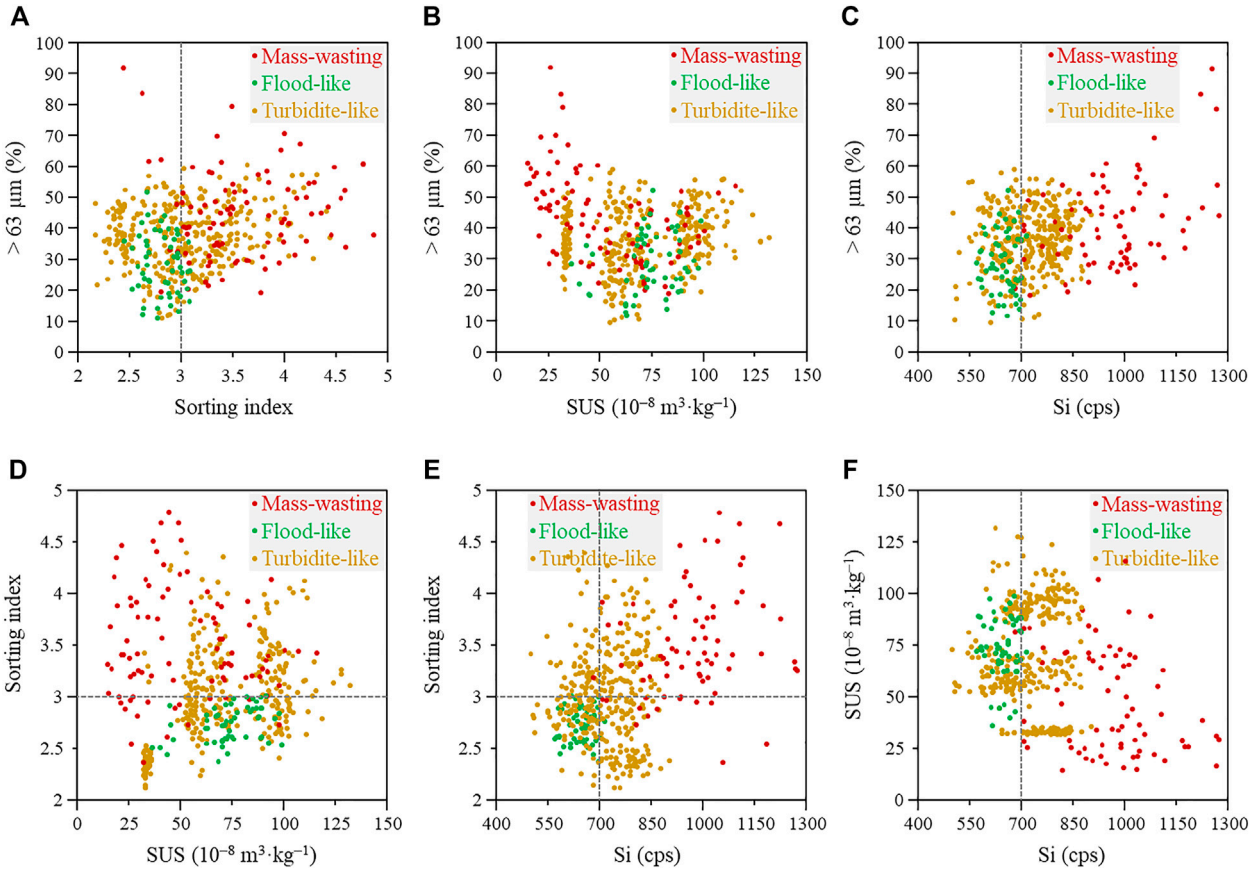

FIGURE 4 | Correlations between **(A)** percentage of >63 μm fraction and sorting index, **(B)** percentage of >63 μm fraction and SUS, **(C)** percentage of >63 μm fraction and Si content, **(D)** sorting index and SUS, **(E)** sorting index and Si content, and **(F)** SUS and Si content of the mass-wasting deposits, flood-like deposits and turbidite-like deposits from the Y20B core.

Sedimentary Proxies

There is no overall trend up the core in the variations of percentages of grain-size fractions, sorting index, SUS, major elemental contents or Rb/Sr ratio of the Y20B core (**Figure 3**). The average percentages of >63, 4–63 and <4 μm fractions are 24.7%, 69.3% and 6.0%, respectively. Sorting index and SUS have average values of 2.9 and 66.9 × 10^{-8} m^3 kg^{-1}, respectively. The average contents of Si, K, Ti, Zr, Mn and Ca are 721, 3,522, 2,617, 778, 940 and 10,696 counts per second (cps), respectively. Rb/Sr ratios and TIC contents have averages of 0.46% and 0.77%, respectively. There are a total of 32 horizons characterized by significantly high percentages of the >63 μm fraction (minimum peak value exceeds 30%). Among them, six horizons (red bars in **Figure 3**) correspond to the mass-wasting deposits (**Figures 2C–H**) and six other horizons correspond to the flood-like deposits (green bars in **Figure 3**). The remaining 20 horizons are turbidite-like deposits (yellow bars in **Figure 3**), generally characterized by abrupt increases in the percentages of >63 μm fraction at the bottom and gradual decreases upwards. The mass-wasting deposits also have remarkably high sorting indices (generally higher than 3) (high sorting indices indicate poor sorting of sediments), low SUS values (minimum valley value is only 14 × 10^{-8} m^3 kg^{-1}) and high Si contents (generally higher than 700 cps with minimum peak value exceeding 890 cps) (**Figures 2C–H**, **3**, **4**). In addition, PCA F1 and F2 account for 43.4% and 19.8% of the total variance within the elemental dataset of the Y20B core, respectively (**Figure 5A**). Three clusters can be defined: the first is dominated by Si, representing a quartz origin; the second is controlled by Ca and Sr, reflecting a plagioclase and/or carbonate origin; and the third is composed of K and other terrigenous elements (Ti, Fe, Rb, Mn, Al and Zr), with the K likely related to a K-feldspar origin (**Figure 5A**). The mass-wasting deposits have PCA F2 values generally lower than zero, and possess the minimum values of both PCA F1 (–12) and F2 (–4.9) throughout the Y20B core (**Figure 5B**). In contrast, the flood-like deposits have relatively low sorting indices (generally lower than 3), low Si contents (generally lower than 700 cps), and relatively high PCA F2 values (generally higher than zero) (**Figures 2K**, **3–5**). The turbidite-like deposits have wide ranging sorting indices (2.1–4.1) and Si contents (497–868 cps) (**Figures 3**, **4**), and have PCA F2 values generally lower than zero when their sorting index is higher than 3 (**Figure 5B**).

The Y20A core has ranges of mean grain size (Mz), percentages of >63 μm fraction, and Si content from 9.1 to

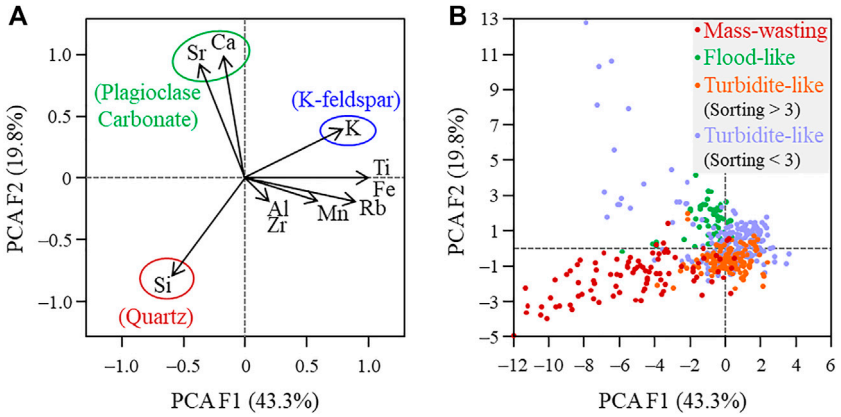

FIGURE 5 | (A) Variables factor map and **(B)** individuals factor map for principal component analysis (PCA) performed on the standardized elemental data of the Y20B core.

321.4 μm, 0%–79.8%, and 193–1376 cps, respectively (**Supplementary Figure S3**). The 260–158 cm depths of the Y20A core is characterized by relatively high values and decreasing trends of Mz, percentages of >63 μm fraction and Si content, equivalent to the 70–40 cm depths of the Y20B core (orange bar in **Supplementary Figure S3**). The peak values of Mz and Si content at 254 cm within the Y20A core correspond to those at 65.5 cm within the Y20B core (**Supplementary Figure S3**). The radiocarbon sampling depths of 198 and 264 cm within the Y20A core can be cautiously correlated with the depths of 50 and 72 cm within the Y20B core, respectively (**Supplementary Figure S3**). The upper 2 cm of the Y20B core, the upper 5 cm of the Y19 core, and the upper 2.5 cm of the Y20 core can be confidently correlated with one other (**Supplementary Figure S3**). The age at 5 cm depth within the Y19 core is 1931 AD, corresponding to the 11 August 1931 M_s 8.0 Fuyun earthquake (Fan et al., 2020b); therefore, the age at 2 cm depth within the Y20B core can also be inferred as 1931 AD (**Supplementary Figure S3**).

DISCUSSION

Sedimentary Record of Paleoearthquakes

Subaquatic faults are present in Yileimu Lake (**Supplementary Figures S1A–D**). These subaquatic faults should not be parts of the Fuyun Fault (**Figure 1A**, **Supplementary Figure S1A**). They were probably produced by seismic shaking from the Fuyun Fault, because the Fuyun Fault was the most active fault in the study area, and the lake was bounded by the Fuyun Fault (**Figure 1A**). The existence of these subaquatic faults suggests that the lake sediments are very sensitive to local seismic activities. However, there may be differences in the sedimentary response to seismicity in different areas of the lake. The Y20B core is located near a subaquatic fault in the nearshore zone of Yileimu Lake (**Figure 1B**, **Supplementary Figure S1B**), potentially representing a promising site to record past earthquakes. The Y20A core is located in the depocenter of Yileimu Lake (**Figure 1B**, **Supplementary Figure S1C**), a location characterized by a flat lake floor and lack of coarse sediments.

Soft-sediment deformation structures (SSDS) in lake sediments (deformed sediments relative to the background sediments) can be triggered by co-seismic (Sims, 1973) and non-seismic processes such as gravity (Van Daele et al., 2014) and wave loading (Migeon et al., 2017). Yileimu Lake is bounded by the Fuyun Fault which produced at least 4 prehistoric $M_s \geq 8.0$ earthquakes (Klinger et al., 2011), and the SSDS consisting of linear waves, were related to the 11 August 1931 M_s 8.0 Fuyun earthquake (**Figure 2C**) (Fan et al., 2020b). Some SSDS in the Y20B core contain high-angle micro-faults, a liquefied diaper or convolute structures, linear waves and clastic dykes, and a clastic dyke (**Figures 2D,G,H,J**), comparable to those produced by experimental and historical earthquakes (e.g., Jiang et al., 2016, 2017). Previous studies indicated that micro-faults were related to seismic-induced brittle failure of carbonate mud with a high initial lithification rate and a considerable strength and density shortly after deposition (Monecke et al., 2004 and references therein). The sedimentary layers of micro-faults at 74–68 cm depths of the Y20B core have much higher TIC (carbonate) contents than those of other types of SSDS (**Figures 2C–J**, **3**). These micro-faults can be produced by an oscillatory movement of the water column and surface sediments during seismic shaking (Migeon et al., 2017). Changes in hydrodynamic conditions should have not been responsible for micro-faults, as evidenced by the absence of micro-faults in other layers of the Y20B core, and in lake sediments which experienced significant changes in hydrodynamic conditions and hardly affected by seismic activities in North China (e.g., Fan et al., 2019). Convolute structures were complex forms of load structures and interpreted as a combination of bulk-density heterogeneities and fluidization associated with water-escape structures during seismic shaking (Suter et al., 2011 and references therein). Linear waves were considered as the results of horizontal movement with different velocities of the laminated layers at water–sediment interfaces, associated with the occurrence of shear energy induced by earthquakes (Lu et al., 2020; Wetzler et al., 2010). Clastic dykes were interpreted as the

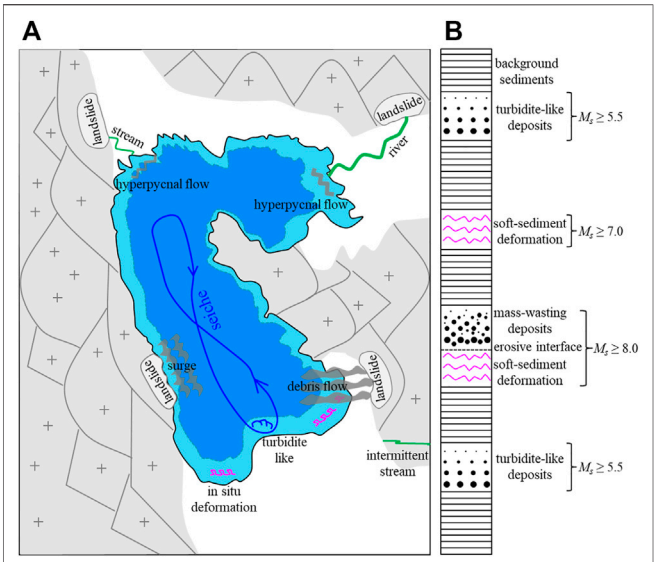

FIGURE 6 | A conceptual model showing **(A)** sedimentary processes in response to seismic shaking and **(B)** earthquake imprints on a sediment core from the nearshore zone of the lake. Mass-wasting deposits include sediments transported by debris flows and hyperpycnal flows.

infillings of hydrofractures during the upward escape of seismic-induced fluidized sediments, when water pressures in the basal layer exceeded the overlying layer (Chen et al., 2009; Moretti, 2000). Therefore, the repeated occurrence of SSDS in the sediments of Yileimu Lake is most likely seismic origin (**Figures 6A,B**). The co-occurrence of some SSDS at the corresponding depths of the Y20A and Y20B cores (**Supplementary Figures S2, S3**) provides support for seismic origin of these widely distributed SSDS in Yileimu Lake. In contrast, gravity-induced SSDS should produce a dominant and regular direction of clastic materials (Van Daele et al., 2014), and wave loading-induced SSDS should produce parallel or regular cross bedding (Beck, 2009; Migeon et al., 2017). There are a total of 9 distinct horizons of SSDS in the Y20B core (**Figures 2C–J**), with each separated by non-seismic horizontal laminations (e.g., **Figure 2J**), indicating 9 past earthquakes originating from the Fuyun Fault (E1–E5, E7, E10, E15 and E19 in **Figure 7**).

Mass-wasting deposits in sediments from small lakes in tectonically active regions were interpreted as the products of coseismic landslides and/or subaqueous slope failures (e.g., Howarth et al., 2014; Lu et al., 2017; Van Daele et al., 2017). In order to distinguish landslide-related deposits from those subaqueous origins in Yileimu Lake, mass-wasting deposits are regarded only as post-seismic deposits from landslides in the lake catchment in this study. Mass-wasting deposits were commonly seen in sediments from small lakes in tectonically active regions (e.g., Howarth et al., 2014; Oswald et al., 2021). The 6 horizons of mass-wasting deposits in the Y20B core consist of poorly sorted sand and scattered, irregularly shaped gravel, and have no Bouma divisions or signs of bioturbation (**Figures 2C–H**, **3**, **4**). The mass-wasting deposits in Yileimu Lake can be interpreted as post-seismic deposits transported by debris flows and/or hyperpycnal flows, reflecting coarse sediment fluxes from earthquake-triggered landslides from surrounding high and steep mountains (**Figures 6A,B**) (e.g., Howarth et al., 2012; Moernaut, 2020). The mass-wasting deposits overlying the SSDS in Yileimu Lake (**Figures 2C–H**) supports the seismic origin of landslides in the lake catchment and *in situ* deformations within the lake (e.g., Lu et al., 2021a). The sharp erosive bases at the interfaces of typical mass-wasting deposits and the underlying SSDS (**Figures 2D,E**) may have resulted from the horizontal movement of bottom water in the lake, induced by shear energy during seismic shaking. The mass-wasting deposits at the top of the Y20B core correspond to the 11 August 1931 M_s 8.0 Fuyun earthquake (**Figure 2C**, **Supplementary Figure S3**). The thickness of these deposits is only 1.5 cm, much thinner than the other 5 horizons of mass-wasting deposits (**Figures 2C–H**). Flood events in the 1900s AD may have expanded the size of the lake (Fan et al., 2021), possibly resulting in increasing distance between the site of the Y20B core and landslide sources, and thereby reducing the sediment flux to the core site. Increased water storage in Yileimu Lake after reservoir construction in the 1950s AD (Fan et al., 2020b) may have also reduced the sedimentation rate in the lake. These factors may therefore have reduced the thickness of the mass-wasting deposits related to the 11 August 1931 M_s 8.0 Fuyun earthquake. The flood-like deposits are well sorted and have clear cross-bedding structures (e.g., **Figures 2K**, **3**, **4**), similar to those flood deposits formed in strong hydrodynamic conditions (Benito et al., 2003).

Yileimu Lake is surrounded by hills of granitic rocks on the west and east (**Figure 1B**). The 11 August 1931 M_s 8.0 Fuyun earthquake caused extensive landslides, providing a large amount of siliciclastic-enriched clastic materials in the lake catchment, and thereby producing the Si-enriched mass-wasting deposits at the top of the Y20B core (**Figure 2C**). The other 5 horizons of mass-wasting deposits have even higher Si content than those at the top of the Y20B core (**Figures 2D–H**, **3**), potentially implying more serious landslides caused by prehistoric great earthquakes. Mn content is generally low in the mass-wasting deposits (**Figures 2C–H**, **3**), indicating oxygen-depleted sedimentary environments and rapid accumulation for these post-seismic deposits (Wils et al., 2021). TIC content is generally low and exhibits an increasing trend throughout the Y20B core, and there are no systematic correlations between the Ca and TIC contents (**Figure 3**). Therefore, a large amount of Ca (as well as Sr) should originate from plagioclase in addition to carbonates (**Figure 5A**). Rb/Sr ratio is generally low in the mass-wasting deposits (**Figure 3**), reflecting weak chemical weathering in the lake catchment (Fan et al., 2021). These data indicate that sediment sources for mass-wasting deposition in Yileimu Lake should have mainly been provided by earthquake-related landslides of weakly weathered granitic rocks. Overall, the mass-wasting deposits overlying the SSDS in the Y20B core reflect 6 past earthquakes (E1, E3, E7, E10, E15 and E19 in **Figure 7**).

Lacustrine turbidites are characterized by gradually upward decreasing grain size, and can be produced by earthquake-induced slope failures and/or slumps in tectonically active regions (e.g., Bertrand et al., 2008; Howarth et al., 2021; Moernaut et al., 2014). However, turbidites can also be formed

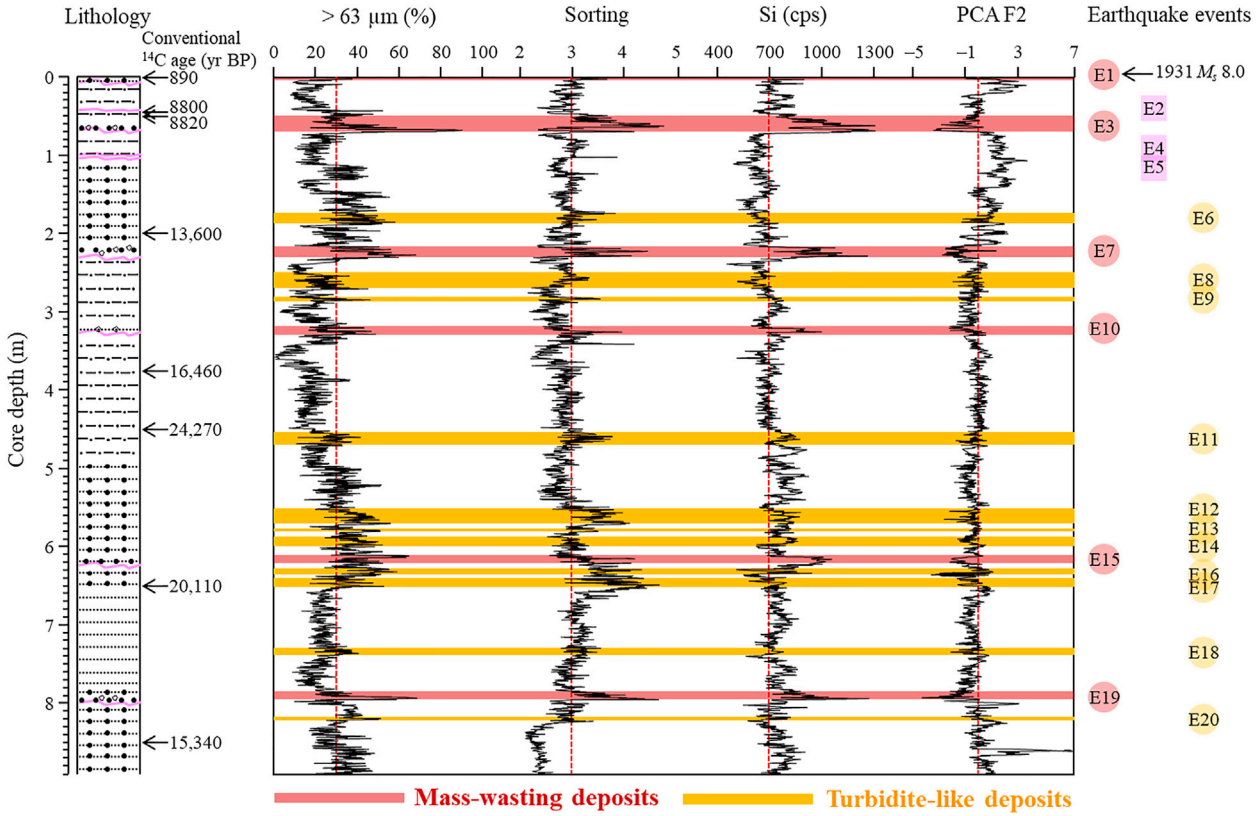

FIGURE 7 | Sedimentary record of past earthquakes inferred from the mass-wasting deposits with underlying SSDS (E1, E3, E7, E10, E15 and E19), isolated SSDS (E2, E4 and E5) and turbidite-like seismites (E6, E8–E9, E11–E14, E16–E18 and E20) from the Y20B core. Lithological legends and conventional ^{14}C ages are same as **Figure 2**.

by flood events (Beck, 2009; Migeon et al., 2017; Praet et al., 2020). Earthquake-related turbidites were commonly characterized by rapidly accumulated and poorly sorted deposits, while flood-induced turbidites were usually well sorted and contain cross-bedding structures and normally graded bedding sequences (Migeon et al., 2017; Moernaut et al., 2014) (e.g., **Figure 2K**). In this study, the deposits having similar grain-size structures to those turbidites are regarded as "turbidite-like" deposits. It is noted that earthquake-induced mass-wasting deposits have sorting indices >3, Si contents >700 cps and PCA F2 < 0 that can be distinguished from flood-like deposits (sorting indices <3, Si contents <700 cps and PCA F2 > 0) in Yileimu Lake (**Figures 3–5**). Therefore, turbidite-like deposits with sorting indices >3, Si contents >700 cps and PCA F2 < 0 are interpreted as seismites in Yileimu Lake (**Figure 7**). When compared with the mass-wasting deposits, the turbidite-like seismites have relatively lower Si contents (**Figures 3**, **4**), implying that the main sediment sources for these turbidite-like seismites were unlikely to be the Si-enriched clastic materials from extensive landslides of granitic rocks in the lake catchment. These turbidite-like seismites may have mainly been related to the re-deposition of nearshore sediments after intense shaking of the lake. Seismic shaking could cause an oscillatory movement of the water column (a seiche effect), and disturb the surface sediments at water-sediment interface (Migeon et al., 2017), resulting in successive re-deposition of sand, silt and clay, forming the turbidite-like deposits. Subaquatic slumps or slope failures within the lake should be secondary factors, because the lake floor is not very steep (**Figure 1B**) (e.g., Schnellmann et al., 2002). The turbidite-like seismites in the Y20B core indicate 11 potential earthquakes (E6, E8–E9, E11–E14, E16–E18 and E20 in **Figure 7**).

Potential Magnitudes for Paleoearthquakes

The 11 August 1931 M_s 8.0 Fuyun earthquake caused extensive landslides of granitic rocks and triggered mass-wasting deposits in the Yileimu Lake catchment (Fan et al., 2020b). Seismic intensity calculation results based on intensity prediction equations (IPEs) from Wang et al. (2000) and Dowrick and Rhoades (2005) were consistent with the published seismic intensity map of the 11 August 1931 M_s 8.0 Fuyun earthquake based on field survey by Shi et al. (2010). These data indicated that an intensity of 8.6 MMI (epicentral distance 50 km) was required for past earthquakes to trigger extensive landslides in the Yileimu Lake catchment (Fan et al., 2020b) (**Figures 8A,B**). Similarly, a minimum intensity of 9 MMI was required for earthquakes produced by the Alpine Fault to cause extensive landslides in the Ellery Lake catchment (Howarth et al., 2016). The small difference of intensity thresholds for landslides in the above two

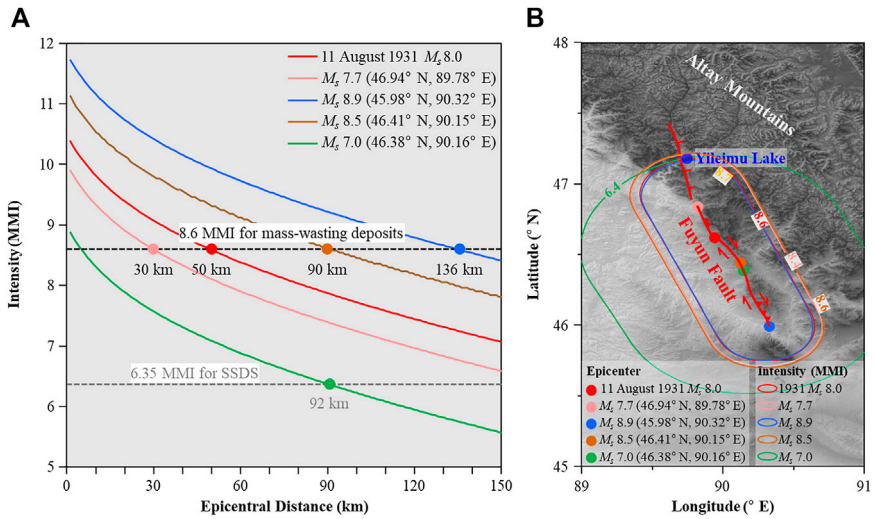

FIGURE 8 | (A) Shaking intensity variations with epicentral distance and **(B)** calibrated isoseismal modelling results for different magnitudes of earthquakes from different sites along the Fuyun Fault. The pink, red, brown, blue and green circles in **(A,B)** are in one-to-one correspondence. The intensity prediction equations (IPEs) used in **(A,B)** are from Wang et al. (2000), and Dowrick and Rhoades (2005), respectively. MMI, Modified Mercalli Intensity.

lake catchments may be related to the different slope angles and rock types. A local intensity of 8.6 MMI in Yileimu Lake could be produced by distant large earthquakes or proximal small earthquakes, making it difficult to determine the magnitudes of prehistoric earthquakes.

The Fuyun Fault is the main seismogenic fault in the study area. It generally consists of a ~50 km-long normal fault segment in the north and a ~120 km-long thrust-slip fault segment in the south (**Figures 1A**, **8B**) (Klinger et al., 2011; Xu et al., 2012). All historical $M_s \geq 7.0$ earthquakes in the study area occurred in the thrust-slip segment (**Figure 1A**). Therefore, it is the southern segment of the Fuyun Fault that seems to have the great potential to trigger large earthquakes. Based on the IPEs from Wang et al. (2000) and Dowrick and Rhoades (2005), an intensity of 8.6 MMI in Yileimu Lake could be generated by an M_s 7.7/8.9 earthquake at the north/south end of the southern fault segment (epicentral distance 30/136 km) in the geological past (**Figures 8A,B**), assuming these earthquakes had similar hypocentral depth, strike, dip and rake to those of the 11 August 1931 M_s 8.0 Fuyun earthquake (Fan et al., 2020b). In addition, characteristic dextral offsets of terraces and stream channels produced by prehistoric $M_s \geq 8.0$ earthquakes from the Fuyun Fault are mainly distributed in the central part of the southern fault segment (Klinger et al., 2011). Hence, it is likely that great earthquakes occurred mainly in the central part of the southern segment of the Fuyun Fault (epicentral distance ~90 km). Therefore, an intensity of 8.6 MMI in Yileimu Lake should be produced by prehistoric $M_s \geq 8.0$ (perhaps M_s 8.5) earthquakes from the Fuyun Fault (**Figures 6B**, **8A**,**B**).

Previous studies suggested that an intensity of 6.5 MMI was required for past earthquakes to produce *in situ* SSDS of linear waves in the Dead Sea, according to the computational fluid dynamics modelling results (Lu et al., 2020). However, these modelling results cannot be simply applied to Yileimu Lake because the lithology, sediment compaction and SSDS in the Y20B core, and the water depth of Yileimu Lake are significantly different from those in Dead Sea. In northern Xinjiang, a minimum intensity of 6.35 MMI could trigger slight SSDS (e.g., linear waves), and an intensity of 7 MMI was able to cause extensive soil liquefaction (Li et al., 2012). Therefore, a local intensity of 6.35 MMI was used as a threshold to trigger SSDS of linear waves in Yileimu Lake. An intensity of 6.35 MMI in Yileimu Lake was likely induced by an $M_s \geq 7.0$ earthquake from the central part of the southern segment of the Fuyun Fault (epicentral distance 92 km) (**Figures 8A,B**). There was no evidence for historical $M_s < 7.0$ earthquakes being able to produce SSDS in the Yileimu Lake catchment (Fan et al., 2020b). In addition, the SSDS of micro-faults (**Figure 2D**), convolute structures (**Figure 2G**) and linear waves and clastic dykes (**Figure 2H**) underlying the mass-wasting deposits in Yileimu Lake, indicates that an intensity of 8.6 MMI (potential $M_s \geq 8.0$ earthquakes) was sufficient to trigger these SSDS. Therefore, the isolated SSDS of linear waves (**Figures 2I,J**) and a clastic dyke (**Figure 2J**) should indicate prehistoric $7.0 \leq M_s < 8.0$ earthquakes (**Figure 6B**).

Turbidite seismites were triggered by a minimum shaking intensity of 5.3–5.7 MMI in Rara Lake in the central Himalaya (Ghazoui et al., 2019). In southern Altay, a historical M_s 5.8 earthquake (epicentral distance 30 km) induced turbidite-like seismites in Yileimu Lake which indicated an intensity threshold of 5.51 MMI (Fan et al., 2020b). In contrast, there was no evidence that historical $M_s < 5.5$ earthquakes could trigger turbidite-like seismites in Yileimu Lake (Fan et al., 2020b). Therefore, a minimum magnitude M_s 5.5 earthquake within a maximum distance of 25 km from Yileimu Lake appears to be required to cause turbidite-like seismites in the lake (**Figure 6B**), based on the IPEs from Wang et al. (2000) and Dowrick and Rhoades (2005). In addition, previous studies suggested a linear

correlation between shaking intensity and turbidite thickness in the south central Chilean lakes (Moernaut et al., 2014). However, distinct lake morphologies and sediment lithology may cause different sedimentary responses to past earthquakes, producing unique intensity thresholds for various turbidites in specific lakes (Moernaut et al., 2014; Lu et al., 2021a). The lack of temporal correlation between historical earthquakes and turbidite-like seismites in Yileimu Lake makes it very difficult to assess the potential magnitudes of prehistoric earthquakes. Since there were no SSDS associated with these turbidite-like seismites, a magnitude M_s < 7.0 was tentatively considered as the maximum threshold.

Timing and Recurrence Behavior of Paleoearthquakes

The ^{14}C age of organic matter from the top of the Y20B core is much older than the sampling date (**Figure 2B**; **Table 1**), possibly reflecting reservoir effects (e.g., Zhou et al., 2009). However, this ^{14}C age is not suitable for calibrating the reservoir effects of the Y20B core, because human- activities (for example, reservoir construction in Yileimu Lake, mine exploitation in Koktokay about 7 km east of Yileimu Lake, and agricultural activities such as grazing in the lacustrine plains) in recent decades (Fuyun County Local Chronicles Compilation Committee, 2003) should have significantly changed the reservoir effects in the shallow water regions of Yileimu Lake. The linearly fitted age–depth curve of the Y20B core shows an intercept of 8,052.1 year (**Supplementary Figure S4**), indicating a potential reservoir effect of thousands of years for the Y20B core. Great earthquake events such as $M_s \geq 8.0$ earthquakes could cause significant changes in the sediments of the whole lake (e.g., Howarth et al., 2014; Wils et al., 2021), allowing for stratigraphic correlations between event layers in the Y20A and Y20B cores (**Supplementary Figure S3**). The branch at 198 cm depth within the Y20A core has a ^{14}C age of 3,090 ± 35 years BP (**Supplementary Figures S2, S3**; **Table 1**). The ^{14}C age of organic matter at 50 cm depth within the Y20B core is 8,820 ± 30 years BP (**Supplementary Figures S2, S3**; **Table 1**). The depth of 198 cm within the Y20A core corresponds to the depth of 50 cm within the Y20B core (**Supplementary Figure S3**), therefore, the age difference between these two corresponding depths (5,730 years) is used as the reservoir correction factor (**Table 1**).

In addition, the linearly fitted age–depth curve of the Y20B core also shows an anomalously old ^{14}C age at 450 cm depth and an anomalously young ^{14}C age at 850 cm depth within the Y20B (**Supplementary Figure S4**; **Table 1**). The sediments at 450 cm depth within the Y20B core were deposited immediately after the earthquake event E11 (**Figure 7**) which may have produced excessive input of old carbon into the lake through remobilization of buried soils in the lake catchment. In addition, the organic matter at 850 cm depth within the Y20B core was very low, and the anomalously young ^{14}C age of organic matter at 850 cm depth within the Y20B core may have been caused by the incorporation of young carbon into the sediments, potentially sourced from near-surface groundwater. Therefore, the ^{14}C ages obtained from 450 to 850 cm depths within the Y20B core are not used. Hence, a total of 7 age data points, including the sampling date of −70 cal year BP at the core top, the ^{14}C ages of the branch and wood at 198 and 264 cm depths within the Y20A core (corresponding to 50 and 72 cm depths within the Y20B core), and the ^{14}C ages of organic matter at 45, 200, 375 and 650 cm depths within the Y20B core, are used in the Bayesian age–depth model. The four ^{14}C ages of organic matter are corrected through subtracting the reservoir correction factor, and then calibrated to the calendar ages (**Figure 9A**; **Table 1**).

The SSDS, mass-wasting deposits and turbidite-like seismites within the Y20B core record a total of 20 potential paleoearthquakes (E1–E20) originating from the Fuyun Fault (**Figure 7**). Post-seismic sediments are rapidly deposited (e.g., Howarth et al., 2014; Avşar et al., 2016; Wils et al., 2021), as evidenced by the almost same ages within the seismites (Fan et al., 2020b). Therefore, the thickness of the mass-wasting deposits and turbidite-like seismites are removed to normalize the depth of the Y20B core. In contrast, the flood-like deposits and the turbidite-like non-seismites are relatively thin and occur frequently; these sediments are not excluded in the age–depth model (Avşar et al., 2015). The Bayesian age–depth model based on the normalized core depth and 7 age data points shows an almost linear curve, indicating that there were no significant discontinuities in the Y20B core, consistent with the lithological characteristics (**Figures 2A,B**). The age–depth model indicates a ^{14}C age of 18.8 cal year BP at 2–0.5 cm depths of the Y20B core, corresponding to the 1931 M_s 8.0 Fuyun earthquake (**Figures 2**, **6**, **9A**,**B**). The Y20B core covers the past 28 kyr (**Figures 9A,B**). The sedimentation rate in the last 3 kyr (~0.15 mm/year) is slightly lower than the preceding period (~0.34 mm/year).

The sedimentary proxies, except for the TIC content, of the Y20B core spanning the past 28 kyr did not exhibit the typical climate fluctuations during the Last Glacial Maximum (LGM)–Deglaciation–Holocene periods (**Figure 3**). The catchment of Yileimu Lake is surrounded by high mountains to the northeast which are covered with perennial snow and ice 3,000 m above sea level (a.s.l.). Therefore, possible snow and ice melting during warming seasons in the geological past may have increased the transport of coarse particles into the lake, concealing the climate characteristics (cold and wet in the LGM and Deglaciation, and warm and dry in the Holocene) of the Westerlies-dominated arid Asia (e.g., Sun et al., 2013), including the Altay region, and reducing the difference in the percentages of >63 μm fraction between the seismic horizon of the E15 event and the adjacent non-seismic horizons (**Figure 7**). The TIC in the Y20B core was mainly from carbonates produced by inorganic precipitation within the lake water, because there were no carbonate rocks in the Yileimu Lake catchment. The TIC contents cannot be ignored throughout the Y20B core (**Figure 3**), implying a dominant subaquatic environment. The Bayesian age–depth model of the Y20A core indicates that the sedimentation rates in the nearshore zone of Yileimu Lake were much lower than those in the depocenter (**Supplementary Figures S2, S3**). This was probably because the depocenter of Yileimu Lake was closer to the rivers entering the lake (**Figure 1B**).

The 6 potential $M_s \geq 8.0$ earthquakes indicated by the mass-wasting deposits overlying SSDS in the Y20B core occurred 15–22, 3,132–3,535, 7,824–9,396, 10,084–11,910, 17,425–20,868 and 22,307–26,665 cal year BP, respectively, based on the Bayesian

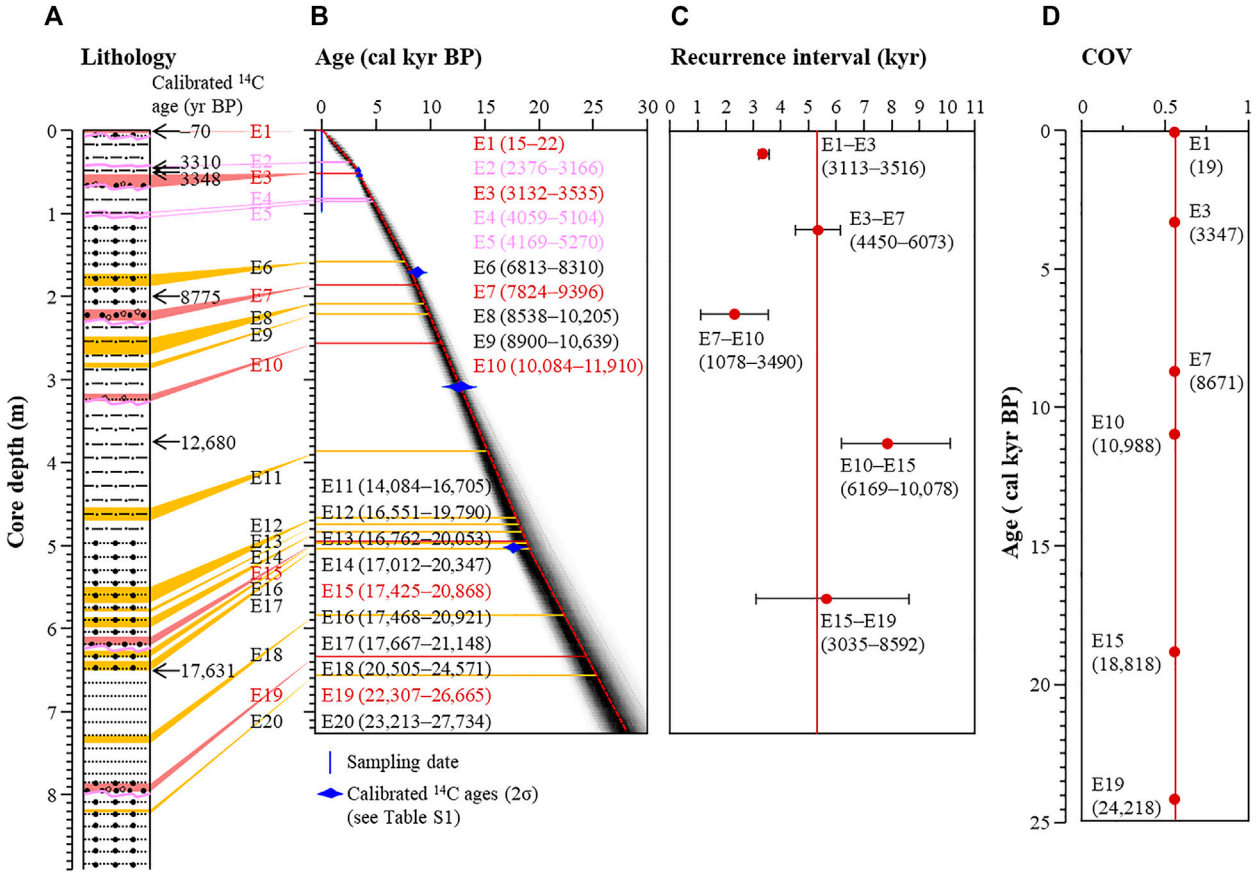

FIGURE 9 | (A) Lithology, calibrated ^{14}C ages and sedimentary record of past earthquakes from the Y20B core. Red and yellow bars indicate the horizons of mass-wasting deposits and turbidite-like seismites, respectively. Lithological legends are same as **Figure 2**. **(B)** Bayesian age–depth model of the Y20B core. Red dashed line indicates weighted mean age. The Bayesian ages (cal year BP) of earthquake events (E1–E20) are given in parentheses. **(C)** Recurrence intervals of potential $M_s \geq 8.0$ earthquakes (E1, E3, E7, E10, E15 and E19). Red circles indicate weighted mean recurrence intervals, and red line indicates average recurrence interval (5,303 years). **(D)** Coefficient of variation (COV) for potential $M_s \geq 8.0$ earthquakes. Red circles indicate weighted mean ages of earthquakes, and red line shows the COV value (0.57).

age-depth model (**Figure 9B**). The recurrence intervals for these earthquakes were between 2,317 and 7,830 years with an average of 5,303 years (**Figure 9C**), much longer than the dating uncertainties (**Figures 9B,C**), and much shorter than the previously published recurrence interval of 9,700 ± 3,300 years for prehistoric $M_s \geq 8.0$ earthquakes originating from the Fuyun Fault (Xu et al., 2012). The timing of these earthquakes was weakly periodic, with a coefficient of variation (COV) of 0.57 (**Figure 9D**) (Moernaut, 2020). The three potential $M_s \geq 7.0$ earthquakes reflected by the three isolated SSDS in the Y20B core occurred 2,376–3,166, 4,059–5,104 and 4,169–5,270 cal year BP, respectively (**Figure 9B**). The minimum recurrence interval of these earthquakes was 110 years, comparable to the previously published interval of 96 years (Fan et al., 2020b). The 11 potential $M_s \geq 5.5$ earthquakes implied by the turbidite-like seismites in the Y20B core occurred between 6,813 and 8,310 and 23,213–27,734 cal year BP, and mainly occurred before 14,084–16,705 cal year BP (**Figure 9B**).

Low sedimentation rate may hinder the identification of sediment features produced by earthquakes with relatively short recurrence intervals (Moernaut et al., 2014). However, a much higher frequency of potential $M_s \geq 7.0$ earthquakes were recorded by the SSDS in the Y20B core over the last 5 kyr, during which time the sedimentation rate of the Y20B core was even lower than the preceding period (**Figure 9B**). Future studies on multi-lake paleoseismic records from different parts of the Fuyun Fault may reveal an even more accurate recurrence pattern of past earthquakes, since small, distant earthquakes (e.g., $M_s \geq 5.5$) may not be recorded in a single lake, and individual lakes with different morphologies, lake levels, sedimentation rates, sediment sources and catchment reliefs may also have different sensitivities to past earthquakes (Moernaut et al., 2014; Hubert-Ferrari et al., 2020; Lu et al., 2021b).

CONCLUSION

Lake sediments in tectonically active regions can provide a complementary paleoseismic record. Widely distributed subaquatic faults in Yileimu Lake, imaged by reflection seismic profiles, indicate that the lake was very sensitive to

past earthquakes originating from the Fuyun Fault. The mass-wasting deposits overlying SSDS in an 890-cm long sediment core from Yileimu Lake reveals six paleoearthquakes with potential magnitudes of $M_s \geq 8.0$, and isolated SSDS reflect three additional potential $M_s \geq 7.0$ paleoearthquakes. Potentially seismic turbidite-like deposits can be distinguished from those with non-seismic origins by sorting indices >3 and Si contents >700 cps. The turbidite-like seismites record 11 potential $M_s \geq 5.5$ paleoearthquakes. Radiocarbon dating and stratigraphic correlations constrain the timing of these past earthquakes to ~28 cal kyr BP. This paleoseismic record suggests a weakly periodic pattern with recurrence intervals between 2,317 and 7,830 years and an average of 5,303 years for potential $M_s \geq 8.0$ earthquakes, and reveals an unprecedented high frequency of potential $M_s \geq 7.0$ earthquakes originating from the Fuyun Fault in the last 5 kyr. These data provide new insights into the recurrence behavior of large earthquakes from intraplate, slow-slipping faults, and highlight the urgent need for an improved assessment of seismic hazards and risks in the Fuyun Fault zone. Future studies on lake sediments with higher sedimentation rates and with wider spatial coverage may help to obtain a more complete paleoseismic record.

DATA AVAILABILITY STATEMENT

The raw data supporting the conclusions of this article will be made available by the authors, without undue reservation.

AUTHOR CONTRIBUTIONS

JF: Conceptualization, data curation, formal analysis, investigation, writing—original draft, writing—review and editing, project administration, resources, supervision. HX: Data curation, investigation, writing—review and editing. WS: data curation, investigation. QG: Data curation, investigation. SZ: Investigation. XW: Data curation. MC: Data curation. SH: Investigation. JW: Data curation. JX: Conceptualization, writing—review and editing.

FUNDING

This study is supported by the National Nonprofit Fundamental Research Grant of China, Institute of Geology, China Earthquake Administration (IGCEA2009).

ACKNOWLEDGMENTS

The authors are grateful to Yin Lu from the Institute of Geology, University of Innsbruck (Innsbruck, Austria) for insightful discussions.

SUPPLEMENTARY MATERIAL

The Supplementary Material for this article can be found online at: https://www.frontiersin.org/articles/10.3389/feart.2022.828801/full#supplementary-material

REFERENCES

Avşar, U., Hubert-Ferrari, A., Batist, M. D., and Fagel, N. (2014). A 3400 Year Lacustrine Paleoseismic Record from the North Anatolian Fault, Turkey: Implications for Bimodal Recurrence Behavior. *Geophys. Res. Lett.* 41, 377–384. doi:10.1002/2013GL058221

Avşar, U., Hubert-Ferrari, A., De Batist, M., Schmidt, S., and Fagel, N. (2015). Sedimentary Records of Past Earthquakes in Boraboy Lake during the Last Ca 600 Years (North Anatolian Fault, Turkey). *Palaeogeogr. Palaeoclimatol. Palaeoecol.* 433, 1–9. doi:10.1016/j.palaeo.2015.04.031

Avşar, U., Jónsson, S., Avşar, Ö., and Schmidt, S. (2016). Earthquake-induced Soft-Sediment Deformations and Seismically Amplified Erosion Rates Recorded in Varved Sediments of Köyceğiz Lake (SW Turkey). *J. Geophys. Res. Solid Earth* 121, 4767–4779. doi:10.1002/2016JB012820

Bai, M. X., Luo, F. Z., Yin, G. H., Xiang, Z. Y., Sheng, J., Shi, S. Z., et al. (1996). Kokotokay—Ertai Active Fault Zone in Xinjiang. *Inl. Earthq.* 10, 319–328. (in Chinese with English abstract). doi:10.16256/j.issn.1001-8956.1996.04.005

Beck, C. (2009). "Late Quaternary Lacustrine Paleo-Seismic Archives in north-western Alps: Examples of Earthquake-Origin Assessment of Sedimentary Disturbances". *Earth-Science Rev.* 96, 327–344. doi:10.1016/j.earscirev.2009.07.005

Benito, G., Sánchez-Moya, Y., and Sopeña, A. (2003). Sedimentology of High-Stage Flood Deposits of the Tagus River, Central Spain. *Sediment. Geology.* 157, 107–132. doi:10.1016/S0037-0738(02)00196-3

Berryman, K. R., Cochran, U. A., Clark, K. J., Biasi, G. P., Langridge, R. M., and Villamor, P. (2012). Major Earthquakes Occur Regularly on an Isolated Plate Boundary Fault. *Science* 336, 1690–1693. doi:10.1126/science.1218959

Bertrand, S., Charlet, F., Chapron, E., Fagel, N., and De Batist, M. (2008). Reconstruction of the Holocene Seismotectonic Activity of the Southern Andes from Seismites Recorded in Lago Icalma, Chile, 39°S. *Palaeogeogr. Palaeoclimatol. Palaeoecol.* 259, 301–322. doi:10.1016/j.palaeo.2007.10.013

Blaauw, M., and Christen, J. A. (2011). Flexible Paleoclimate Age-Depth Models Using an Autoregressive Gamma Process. *Bayesian Anal.* 6, 457–474. doi:10.1214/ba/1339616472

Blott, S. J., and Pye, K. (2001). GRADISTAT: a Grain Size Distribution and Statistics Package for the Analysis of Unconsolidated Sediments. *Earth Surf. Process. Landforms* 26, 1237–1248. doi:10.1002/esp.261

Brock, F., Higham, T., Ditchfield, P., and Ramsey, C. B. (2010). Current Pretreatment Methods for AMS Radiocarbon Dating at the Oxford Radiocarbon Accelerator Unit (Orau). *Radiocarbon* 52, 103–112. doi:10.1017/S0033822200045069

Chen, J., van Loon, A. J., Han, Z., and Chough, S. K. (2009). Funnel-shaped, Breccia-Filled Clastic Dykes in the Late Cambrian Chaomidian Formation (Shandong Province, China). *Sediment. Geology.* 221, 1–6. doi:10.1016/j.sedgeo.2009.09.006

Cui, P., Lin, Y.-m., and Chen, C. (2012). Destruction of Vegetation Due to Geo-Hazards and its Environmental Impacts in the Wenchuan Earthquake Areas. *Ecol. Eng.* 44, 61–69. doi:10.1016/j.ecoleng.2012.03.012

Ding, G. Y. (1985). *The Fuyun Earthquake Fault Zone*. Beijing: Seismological Press. (in Chinese).

Dowrick, D. J., and Rhoades, D. A. (2005). Revised Models for Attenuation of Modified Mercalli Intensity in New Zealand Earthquakes. *Bnzsee* 38, 185–214. doi:10.5459/bnzsee.38.4.185-214

Fan, J., Jiang, H., Shi, W., Guo, Q., Zhang, S., Wei, X., et al. (2021). A 450-year Warming and Wetting Climate in Southern Altay Inferred from a Yileimu Lake Sediment Core. *Quat. Int.* 592, 37–50. doi:10.1016/j.quaint.2021.04.035

Fan, J., Jiang, H., Shi, W., Guo, Q., Zhang, S., Wei, X., et al. (2020b). A 450-year Lacustrine Record of Recurrent Seismic Activities Around the Fuyun Fault, Altay Mountains, Northwest China. *Quat. Int.* 558, 75–88. doi:10.1016/j.quaint.2020.08.051

Fan, J., Wei, X., Shi, W., Guo, Q., Zhang, S., Xu, H., et al. (2020a). Response of Tree Rings to Earthquakes during the Past 350 Years at Jiuzhaigou in the Eastern Tibet. *Sci. Total Environ.* 731, 138714. doi:10.1016/j.scitotenv.2020.138714

Fan, J., Xiao, J., and Qin, X. (2019). Millennial- and Centennial-Scale Droughts at the Northern Margin of the East Asian Summer Monsoon during the Last Deglaciation: Sedimentological Evidence from Dali Lake. *Palaeogeogr. Palaeoclimatol. Palaeoecol.* 514, 361–372. doi:10.1016/j.palaeo.2018.11.001

Fan, J., Xiao, J., Wen, R., Zhang, S., Wang, X., Cui, L., et al. (2016). Droughts in the East Asian Summer Monsoon Margin during the Last 6 Kyrs: Link to the North Atlantic Cooling Events. *Quat. Sci. Rev.* 151, 88–99. doi:10.1016/j.quascirev.2016.09.001

Fuyun County Local Chronicles Compilation Committee (2003). *Annals of Fuyun County*. Urumqi: Volksverlag Xinjiang. (in Chinese).

Ghazoui, Z., Bertrand, S., Vanneste, K., Yokoyama, Y., Nomade, J., Gajurel, A. P., et al. (2019). Potentially Large post-1505 AD Earthquakes in Western Nepal Revealed by a lake Sediment Record. *Nat. Commun.* 10, 2258. doi:10.1038/s41467-019-10093-4

Howarth, J. D., Fitzsimons, S. J., Norris, R. J., and Jacobsen, G. E. (2012). Lake Sediments Record Cycles of Sediment Flux Driven by Large Earthquakes on the Alpine Fault, New Zealand. *Geology* 40, 1091–1094. doi:10.1130/G33486.1

Howarth, J. D., Fitzsimons, S. J., Norris, R. J., and Jacobsen, G. E. (2014). Lake Sediments Record High Intensity Shaking that Provides Insight into the Location and Rupture Length of Large Earthquakes on the Alpine Fault, New Zealand. *Earth Planet. Sci. Lett.* 403, 340–351. doi:10.1016/j.epsl.2014.07.008

Howarth, J. D., Fitzsimons, S. J., Norris, R. J., Langridge, R., and Vandergoes, M. J. (2016). A 2000 Yr Rupture History for the Alpine Fault Derived from Lake Ellery, South Island, New Zealand. *Geol. Soc. America Bull.* 128, 627–643. doi:10.1130/B31300.1

Howarth, J. D., Orpin, A. R., Kaneko, Y., Strachan, L. J., Nodder, S. D., Mountjoy, J. J., et al. (2021). Calibrating the marine Turbidite Palaeoseismometer Using the 2016 Kaikōura Earthquake. *Nat. Geosci.* 14, 161–167. doi:10.1038/s41561-021-00692-6

Hubert-Ferrari, A., Lamair, L., Hage, S., Schmidt, S., Çağatay, M. N., and Avşar, U. (2020). A 3800 Yr Paleoseismic Record (Lake Hazar Sediments, Eastern Turkey): Implications for the East Anatolian Fault Seismic Cycle. *Earth Planet. Sci. Lett.* 538, 116152. doi:10.1016/j.epsl.2020.116152

Jiang, H., Zhong, N., Li, Y., Ma, X., Xu, H., Shi, W., et al. (2017). A Continuous 13.3-ka Record of Seismogenic Dust Events in Lacustrine Sediments in the Eastern Tibetan Plateau. *Sci. Rep.* 7, 15686. doi:10.1038/s41598-017-16027-8

Jiang, H., Zhong, N., Li, Y., Xu, H., Yang, H., and Peng, X. (2016). Soft Sediment Deformation Structures in the Lixian Lacustrine Sediments, Eastern Tibetan Plateau and Implications for Postglacial Seismic Activity. *Sediment. Geology.* 344, 123–134. doi:10.1016/j.sedgeo.2016.06.011

Klinger, Y., Etchebes, M., Tapponnier, P., and Narteau, C. (2011). Characteristic Slip for Five Great Earthquakes along the Fuyun Fault in China. *Nat. Geosci* 4, 389–392. doi:10.1038/NGEO1158

Kremer, K., Gassner-Stamm, G., Grolimund, R., Wirth, S. B., Strasser, M., and Fäh, D. (2020). A Database of Potential Paleoseismic Evidence in Switzerland. *J. Seismol.* 24, 247–262. doi:10.1007/s10950-020-09908-5

Li, Z. Y., Cao, Z. Z., and Li, Y. R. (2012). New Prediction Formula of Sand Liquefied on Bachu-Jiashi Earthquake Survey. *Amm* 170-173, 2880–2884. doi:10.4028/www.scientific.net/AMM.170-173.2880

Lin, A., and Lin, S. j. (1998). Tree Damage and Surface Displacement: The 1931 M 8.0 Fuyun Earthquake. *J. Geology.* 106, 751–758. doi:10.1086/516058

Lu, Y., Moernaut, J., Bookman, R., Waldmann, N., Wetzler, N., Agnon, A., et al. (2021a). A New Approach to Constrain the Seismic Origin for Prehistoric Turbidites as Applied to the Dead Sea Basin. *Geophys. Res. Lett.* 48, e2020GL090947. doi:10.1029/2020GL090947

Lu, Y., Moernaut, J., Waldmann, N., Bookman, R., Ian Alsop, G., Hubert-Ferrari, A., et al. (2021b). Orbital- and Millennial-Scale Changes in Lake-Levels Facilitate Earthquake-Triggered Mass Failures in the Dead Sea Basin. *Geophys. Res. Lett.* 48, e2021GL093391. doi:10.1029/2021GL093391

Lu, Y., Waldmann, N., Alsop, G. I., and Marco, S. (2017). Interpreting Soft Sediment Deformation and Mass Transport Deposits as Seismites in the Dead Sea Depocenter. *J. Geophys. Res. Solid Earth* 122, 8305–8325. doi:10.1002/2017JB014342

Lu, Y., Wetzler, N., Waldmann, N., Agnon, A., Biasi, G. P., and Marco, S. (2020). A 220,000-Year-Long Continuous Large Earthquake Record on a Slow-Slipping Plate Boundary. *Sci. Adv.* 6, eaba4170. doi:10.1126/sciadv.aba4170

Migeon, S., Garibaldi, C., Ratzov, G., Schmidt, S., Collot, J.-Y., Zaragosi, S., et al. (2017). Earthquake-triggered Deposits in the Subduction Trench of the north Ecuador/south Colombia Margin and Their Implication for Paleoseismology. *Mar. Geology.* 384, 47–62. doi:10.1016/j.margeo.2016.09.008

Moernaut, J., Daele, M. V., Heirman, K., Fontijn, K., Strasser, M., Pino, M., et al. (2014). Lacustrine Turbidites as a Tool for Quantitative Earthquake Reconstruction: New Evidence for a Variable Rupture Mode in South central Chile. *J. Geophys. Res. Solid Earth* 119, 1607–1633. doi:10.1002/2013JB010738

Moernaut, J. (2020). Time-dependent Recurrence of strong Earthquake Shaking Near Plate Boundaries: A lake Sediment Perspective. *Earth-Science Rev.* 210, 103344. doi:10.1016/j.earscirev.2020.103344

Moernaut, J., Van Daele, M., Fontijn, K., Heirman, K., Kempf, P., Pino, M., et al. (2018). Larger Earthquakes Recur More Periodically: New Insights in the Megathrust Earthquake Cycle from Lacustrine Turbidite Records in South-central Chile. *Earth Planet. Sci. Lett.* 481, 9–19. doi:10.1016/j.epsl.2017.10.016

Monecke, K., Anselmetti, F. S., Becker, A., Sturm, M., and Giardini, D. (2004). The Record of Historic Earthquakes in lake Sediments of Central Switzerland. *Tectonophysics* 394, 21–40. doi:10.1016/j.tecto.2004.07.053

Moretti, M. (2000). Soft-sediment Deformation Structures Interpreted as Seismites in Middle-Late Pleistocene Aeolian Deposits (Apulian Foreland, Southern Italy). *Sediment. Geology.* 135, 167–179. doi:10.1016/S0037-0738(00)00070-1

Oswald, P., Strasser, M., Hammerl, C., and Moernaut, J. (2021). Seismic Control of Large Prehistoric Rockslides in the Eastern Alps. *Nat. Commun.* 12, 1059. doi:10.1038/s41467-021-21327-9

Pollitz, F., Vergnolle, M., and Calais, E. (2003). Fault Interaction and Stress Triggering of Twentieth century Earthquakes in Mongolia. *J. Geophys. Res.* 108, 2503. doi:10.1029/2002JB002375

Praet, N., Van Daele, M., Collart, T., Moernaut, J., Vandekerkhove, E., Kempf, P., et al. (2020). Turbidite Stratigraphy in Proglacial Lakes: Deciphering Trigger Mechanisms Using a Statistical Approach. *Sedimentology* 67, 2332–2359. doi:10.1111/sed.12703

Ramsey, C. B., and Lee, S. (2013). Recent and Planned Developments of the Program OxCal. *Radiocarbon* 55, 720–730. doi:10.1017/S0033822200057878

Reimer, P. J., Austin, W. E. N., Bard, E., Bayliss, A., Blackwell, P. G., Bronk Ramsey, C., et al. (2020). The IntCal20 Northern Hemisphere Radiocarbon Age Calibration Curve (0-55 Cal kBP). *Radiocarbon* 62, 725–757. doi:10.1017/RDC.2020.41

Schnellmann, M., Anselmetti, F. S., Giardini, D., McKenzie, J. A., and Ward, S. N. (2002). Prehistoric Earthquake History Revealed by Lacustrine Slump Deposits. *Geol* 30, 1131–1134. doi:10.1130/0091-7613(2002)030<1131:PEHRBL>2.0.CO;2

Shen, J., Li, Y. Z., Wang, Y. P., and Song, F. M. (2003). The Active Faults in Altai Mountains. *Earth Sci. Front.* 10, 132–141. (in Chinese with English abstract). doi:10.3321/j.issn:1005-2321.2003.z1.020

Shi, J., Shen, J., Bai, M. X., and Shi, G. L. (2010). Intensity Image Revision on Fuyun 8.0 Earthquake on Aug. 11, 1931 in Xinjiang. *Inland Earthq* 24, 37–40. (in Chinese with English abstract). doi:10.3969/j.issn.1001-8956.2010.01.007

Sims, J. D. (1973). Earthquake-induced Structures in Sediments of Van Norman Lake, San Fernando, California. *Science* 182, 161–163. doi:10.1126/science.182.4108.161

Strasser, M., Anselmetti, F. S., Fäh, D., Giardini, D., and Schnellmann, M. (2006). Magnitudes and Source Areas of Large Prehistoric Northern Alpine Earthquakes Revealed by Slope Failures in Lakes. *Geol* 34, 1005–1008. doi:10.1130/G22784A.1

Sullivan, K. M., and Hossain, S. M. M. (2010). Earthquake Mortality in Pakistan. *Disasters* 34, 176–183. doi:10.1111/j.1467-7717.2009.01121.x

Sun, A., Feng, Z., Ran, M., and Zhang, C. (2013). Pollen-recorded Bioclimatic Variations of the Last ~22,600 Years Retrieved from Achit Nuur Core in the

Western Mongolian Plateau. *Quat. Int.* 311, 36–43. doi:10.1016/j.quaint.2013.07.002

Suter, F., Martínez, J. I., and Vélez, M. I. (2011). Holocene Soft-Sediment Deformation of the Santa Fe-Sopetrán Basin, Northern Colombian Andes: Evidence for Pre-hispanic Seismic Activity? *Sediment. Geology.* 235, 188–199. doi:10.1016/j.sedgeo.2010.09.018

Van Daele, M., Cnudde, V., Duyck, P., Pino, M., Urrutia, R., and De Batist, M. (2014). Multidirectional, Synchronously-Triggered Seismo-Turbidites and Debrites Revealed by X-ray Computed Tomography (CT). *Sedimentology* 61, 861–880. doi:10.1111/sed.12070

Van Daele, M., Meyer, I., Moernaut, J., De Decker, S., Verschuren, D., and De Batist, M. (2017). A Revised Classification and Terminology for Stacked and Amalgamated Turbidites in Environments Dominated by (Hemi)pelagic Sedimentation. *Sediment. Geology.* 357, 72–82. doi:10.1016/j.sedgeo.2017.06.007

Vanholder, R., Sever, M. S., De Smet, M., Erek, E., and Lameire, N. (2001). Intervention of the Renal Disaster Relief Task Force in the 1999 Marmara, Turkey Earthquake. *Kidney Int.* 59, 783–791. doi:10.1046/j.1523-1755.2001.059002783.x

Wang, S. Y., Yu, Y. X., Gao, A. J., and Yan, X. J. (2000). Development of Attenuation Relations for Ground Motion in China. *Earthq. Res. CHN.* 16, 99–106. (in Chinese with English abstract). doi:10.3969/j.issn.1001-4683.2000.02.001

Wetzler, N., Marco, S., and Heifetz, E. (2010). Quantitative Analysis of Seismogenic Shear-Induced Turbulence in lake Sediments. *Geology* 38, 303–306. doi:10.1130/G30685.1

Wils, K., Daryono, M. R., Praet, N., Santoso, A. B., Dianto, A., Schmidt, S., et al. (2021). The Sediments of Lake Singkarak and Lake Maninjau in West Sumatra Reveal Their Earthquake, Volcanic and Rainfall History. *Sediment. Geology.* 416, 105863. doi:10.1016/j.sedgeo.2021.105863

Xu, X., and Deng, Q. (1996). Nonlinear Characteristics of Paleoseismicity in China. *J. Geophys. Res.* 101, 6209–6231. doi:10.1029/95JB01238

Xu, X. W., Sun, X. Z., Tan, X. B., Li, K., Yu, G. H., Etchebes, M., et al. (2012). Fuyun Fault: Long-Term Faulting Behavior under Low Crustal Strain Rate. *Seismol. Geol.* 34, 606–617. (in Chinese with English abstract). doi:10.3969/j.issn.0253-4967.2012.04.007

Zhou, A.-f., Chen, F.-h., Wang, Z.-l., Yang, M.-l., Qiang, M.-r., and Zhang, J.-w. (2009). Temporal Change of Radiocarbon Reservoir Effect in Sugan Lake, Northwest China during the Late Holocene. *Radiocarbon* 51, 529–535. doi:10.1017/S0033822200055909

Conflict of Interest: The authors declare that the research was conducted in the absence of any commercial or financial relationships that could be construed as a potential conflict of interest.

Publisher's Note: All claims expressed in this article are solely those of the authors and do not necessarily represent those of their affiliated organizations, or those of the publisher, the editors and the reviewers. Any product that may be evaluated in this article, or claim that may be made by its manufacturer, is not guaranteed or endorsed by the publisher.